Study of the effect of Compression Ratio of a Variable Compression Ratio Diesel Engine fuelled with Jatropha oil blend with diesel

Biswajit De (India), Raj SeKhar Panua (India)

Abstract

Biodiesel have proven to be most promising of various alternate fuels used in diesel engine to reduced exhaust emissions maintaining the performance characteristics. The emission & performance characteristics are also affected by various working parameters like compression ratio, injection pressure and injection timing. In the present study optimum compression ratio for variable compression ratio diesel engine fuelled with Jatropha oil blends with diesel (20%) has been determined at 203 bars injector opening pressure , 23^0 CA BTDC injection timing and at 1500 rev/min rated speed. The test results revealed that compression ratio 19 exhibited better performance and lower emissions compared to mineral diesel fuel and hence, is considered as optimum compression ratio.

Keywords: Variable compression ratio engine; optimum; blend; emissions; performance;

Available online at www.sciencedirect.com

ScienceDirect

Procedia Engineering 00 (2015) 000–000

Procedia Engineering

www.elsevier.com/locate/procedia

6th BSME International Conference on Thermal Engineering (ICTE 2014)

Numerical modeling of Biomass co-combustion with pulverized coal in a small scale furnace

Arafat A. Bhuiyan and Jamal Naser*

Faculty of Science, Engineering and Technology (FSET)
Swinburne University of Technology, VIC-3122, Australia

Abstract

Co-combustion of Biomass is a promising greenhouse gases (GHG) abatement technology. This study presents a numerical modeling of co-combustion of coal and Biomass firing under air and oxy-fuel conditions in a small scale furnace. Co-firing conditions are varied with the Biomass sharing considering 20%, 40% on mass basis. Level of confidence is achieved by comparing the model-predicted peak radiative heat flux against the experimental data. Results are presented comparing the flame temperature distribution, species concentration for different cases. Unburned Carbon in ash (CIA) is predicted for different cases and reasonable agreement has been obtained. An improved burnout was observed in oxy-fuel cases. No significant change in CO_2 concentrations with the increase of biomass contribution to the total fuel input proves that biomass is CO_2-neutral energy source.

Peer-review under responsibility of organizing committee of the 6th BSME International Conference on Thermal Engineering (ICTE 2014).

Keywords: Co-combustion, Biomass, Oxy-fuel, Carbon in ash (CIA), Recycled Ratio (RR), Computational Fluid Dynamics (CFD).

1. Introduction

Co-combustion of Biomass with coal deals significant option for the reduction of greenhouse gas emissions specially the reduction of carbon dioxide (CO_2) emissions [1]. Co-combustion of Biomass with fossil fuel also increase the use of renewable based energy sources in energy systems [2]. On the other hand, oxy-fuel combustion is a proven carbon capturing technology [3]. In order to increase the CO_2 capture efficiency, the combination of oxy-

* Corresponding author. Tel.: +61 3 9214 8655; fax: +61 3 9214 8264.
E-mail address: jnaser@swin.edu.au

Peer-review under responsibility of organizing committee of the 6th BSME International Conference on Thermal Engineering (ICTE 2014).

fuel technology with Biomass co-firing is an interesting scope to investigate. In recent years, many efforts have been conducted to investigate the effects of co-combustion of various types of Biomass in the existing small and large scale industrial furnace [1, 4-7]. Those results showed that co-combustion is technically feasible provided that agglomeration problems could be confronted. It is essential to model co-combustion in order to discover potential problems that may occur during Biomass co-firing and to mitigate potential negative effects of Biomass, including lower efficiency due to lower burnout. In this study, a comprehensive investigation has been carried out considering co-combustion of biofuel with coal under air-fuel and oxy-fuel conditions in a small scale furnace using a commercial computational fluid dynamics code AVL Fire ver.2009.2.

2. Model description and methodology

2.1. Geometry and operating condition of the boiler

This computational fluid dynamics (CFD) study is conducted simulating a small scale furnace. The dimensions and specifications of this refractory lined furnace are given in details in [8-10]. The furnace is equipped by an aerodynamically air staged burner with swirling facilities for proper mixing of the fuel and oxidizers [11]. Figure 1 shows the schematic representation of the combustion test facility used in this numerical study. In this study, Shea meal as a Biomass is co-fired with Russian coal as in the experiment [8]. The fuels properties are given in Table 1. Different co-firing ratios are considered on mass basis such as 20% and 40% Biomass sharing. Different oxy-fuel conditions are studied based on recycled ratios (RR) and compared with the air-firing case. Total three RR cases are considered in the range of 68-75%. The details of the applied boundary conditions are given in Table 2. The fuel particles size ranges in 75µm ->300µm for both fuels. But, larger particles are comparatively higher in biomass fuel.

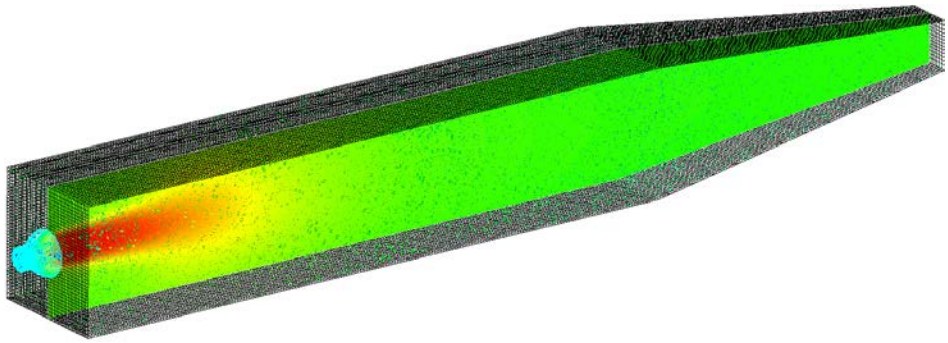

Figure 1: Schematic representation of the combustion test facility used in the numerical study.

Table 1: Proximate and ultimate analysis of the used fuels

Fuel	Proximate analysis, (% as received)				Ultimate analysis, (% as received)					GCV MJ/kg
	VM	FC	Ash	Moisture	C	H	N	S	O	
Coal	33.55	48.27	11.98	6.23	65.91	4.59	2.09	0.34	8.89	27.098
Biomass	56.47	27.26	4.72	11.58	44.58	5.88	2.60	0.24	38.43	17.362

Table 2: Inlet Boundary condition applied to the burner

Flow parameters	Primary Oxidizer				Secondary Oxidizer			
	Air	RR75	RR72	RR68	Air	RR75	RR72	RR68
Gas flow, kg/h	110	155	155	155	620	600	512	424
Gas Temperature, K	343	343	343	343	543	543	543	543
O2 fraction, (kg/kg)	23.3	16.2	16.2	16.2	23.3	22.8	25.4	32.5

2.2. Numerical description

In this study, CFD is the main workhorse. The details numerical modeling used in this study are based on one of the author's previous work [12-17]. The mathematical model includes Eulerian-lagrangian gas and particulate phase modelling. In fuels combustion modelling, two important processes called devolatilisation and char oxidation are written as user-defined routines having different kinematics and coupled with the CFD code. In this study, Biomass particles are assumed in irregular shape while coal particles are assumed as spherical particle. In order to consider these effects, proper aerodynamics of the irregular shaped particles is taken into account by a user-defined drag correlation given in [18]. Regarding turbulence, k-ε turbulence model is considered. The reaction rate is determined by the Eddy-Breakup model [19]. In case of chemical reactions, multi-steps mechanisms have been introduced. For devolatilisation process, three steps homogeneous reactions are considered, but for char oxidation process, two-steps heterogeneous reaction mechanism is applied. In this study, SIMPLE algorithm is used for pressure velocity coupling. A standard convergence criterion of absolute residual 10^{-4} is considered. For the total duration of 80 s, time steps 0.0025 s was settled and the results were averaged after achieving quasi-steady state for all the variables. A 3-D non-uniform structured grid with 650,000 cells was adopted for the study.

3. Results and discussion

In this study, three different recycled ratios (RR) have been considered such as RR68, RR72 and RR75 cases. Results were presented and compared with the air-firing case. The effects of Biomass shares in co-firing (20% and 40% sharing of Biomass), firing conditions (see Table 2), and different fuels properties (see Table 1) have significant contribution to the overall performance of the furnace that are investigated and discussed in the following sections. For validation of the numerical work, peak radiative heat flux were predicted for different cases and compared with the available experimental work [8]. The comparison of the numerical and experimental peak radiative heat transfer measurement were presented in Table 5. It is found that the error percentage is very low in most of the cases.

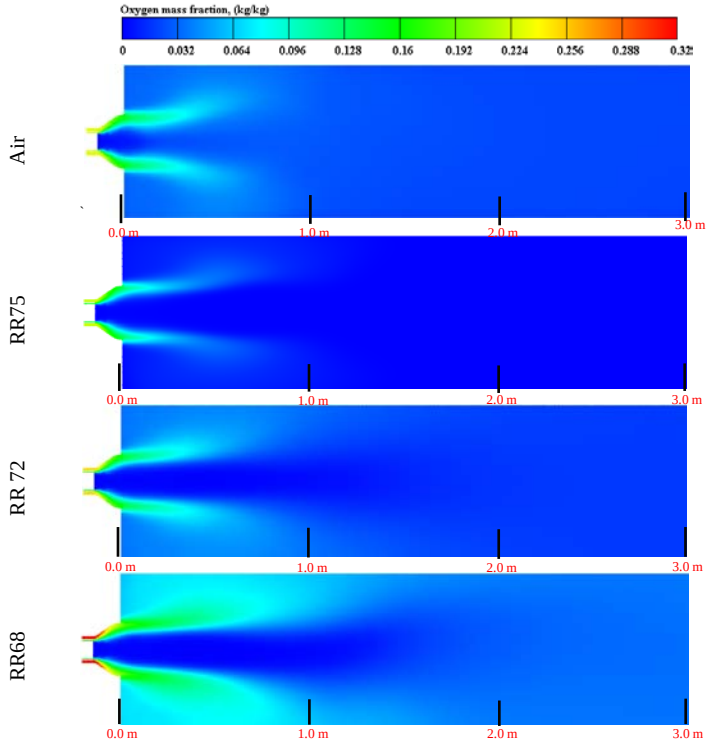

Figure 2: Oxygen mass fraction distribution on the horizontal plane for different cases considered (40% Biomass sharing).

Table 3: Comparison of numerical and experimental peak radiative heat transfer measurement

Cases	Coal+20% Biomass			Coal+40% Biomass		
	Experiment, KW/m^2	Prediction, KW/m^2	Error, %	Experiment, KW/m^2	Prediction, KW/m^2	Error, %
Air	385	395.36	2.69	395	360.56	8.71
RR75	328	318.90	2.77	--	294.77	--
RR72	375	380.97	1.59	328	340.99	3.96
RR68	435	437.85	0.65	370	386.67	4.50

Table 4: Prediction of numerical mean and furnace exit temperature for different cases

Cases	Coal+20% Biomass		Coal+40% Biomass	
	Mean Temp, K	Exit Temp, K	Mean Temp, K	Exit Temp, K
Air	1655.76	1338.62	1618.26	1333.26
RR75	1639.10	1328.94	1621.30	1328.94
RR72	1676.50	1332.38	1667.00	1328.16
RR68	1765.00	1422.70	1750.00	1414.65

The distributions of major oxidizing element (O_2) for different cases are presented in figure 2. From the figure, it is found that the peak value of the O_2 mass fraction is observed in the burner area. The maximum O_2 mass fraction in RR68 case is approximately 0.32 kg/kg. It is also seen that with the decrease of recycled ratio (RR), the mass fraction of O_2 is increased. This is in line with the applied boundary condition in table 2. As oxygen (O_2) mass fraction in increasing, accurate mixing of the fuels particle with the oxidizer is achieved, thus complete devolatilisation occurred. After devolatilisation, remaining amount of O_2 element reacts slowly with the char particle. This is the reason to form higher flame temperature having higher O_2 mass fraction in lower RR cases.

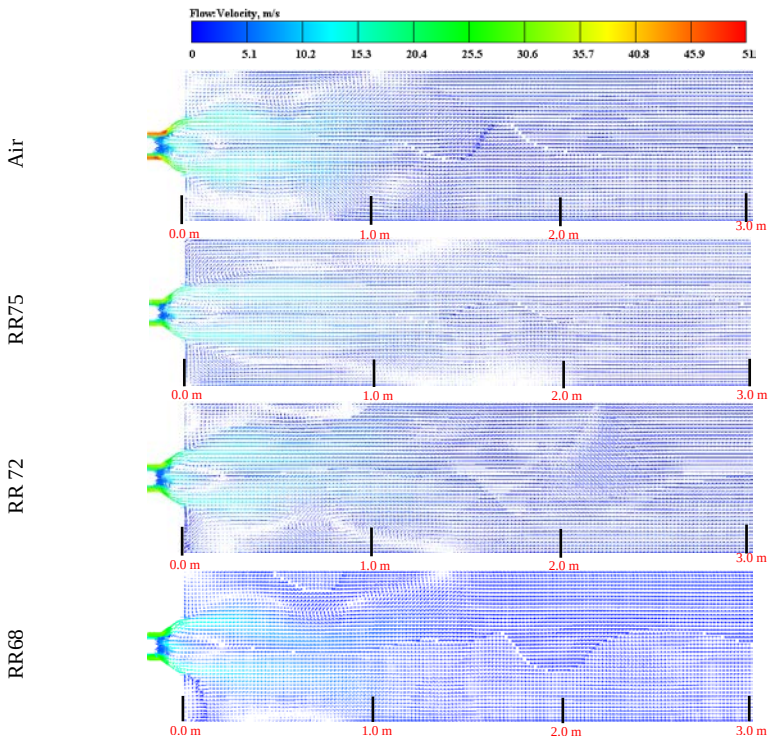

Figure 3: Axial velocity distribution (m/s) on the horizontal plane for different cases considered (40% Biomass sharing)

Axial velocity distributions for different cases considered in this study are presented in figure 3. This figure is representing for 40% sharing of Biomass co-combustion. From this figure, it is found that there are reaction zone after the exit of the burner where flames are expected to be found. Also, some internal and external recirculation zones are observed in various positions for all the cases. The position of external recirculation zone varies due to variation of flow conditions presented in table 2.With the increase of RR, flow velocity is increased, which will permit the fuel particles passing the reaction zone quickly. With the decrease of RR, flow becomes low which allow the fuel to stay in the reaction zone in more time. Thus volatile matters burn completely resulting higher flame temperature in lower RR.

The flame temperature distributions for different co-combustion ratio under different combustion environment on horizontal plane along the center of the furnace are presented in figures 4-7. These figures highlight the effects of variation of Biomass sharing in respective combustion cases. Biomass contains higher volatile contents compared to coal. So, in case of air-firing, Biomass burns early in the furnace because of the presence of highly volatile matters. With the increase of Biomass sharing in 40% case, the flame temperature expands more compared to 20% sharing because of higher percentage of volatile contents for all the cases. Though higher amount of volatile contents correspond to larger volume of flame in RR cases, but higher moisture content and larger particle sizes of Biomass tend to decrease the peak flame temperature. In this study, furnace exit temperature are predicted at a position of 4.2m from burner exit while mean flame temperature are predicted at 0.3m from burner exit. The furnace exit temperature and mean flame temperatures for different cases considering different Biomass sharing are presented in table 4. With the decrease of RR, mean flame temperature and furnace exit temperature increases. While considering increase of Biomass sharing from 20% to 40%, all the temperatures are lower in respective cases.

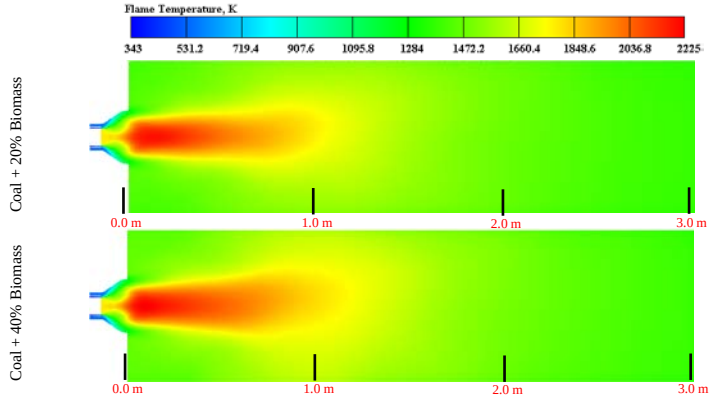

Figure 4: Flame temperature distribution on the horizontal plane for different Biomass sharing under air firing case.

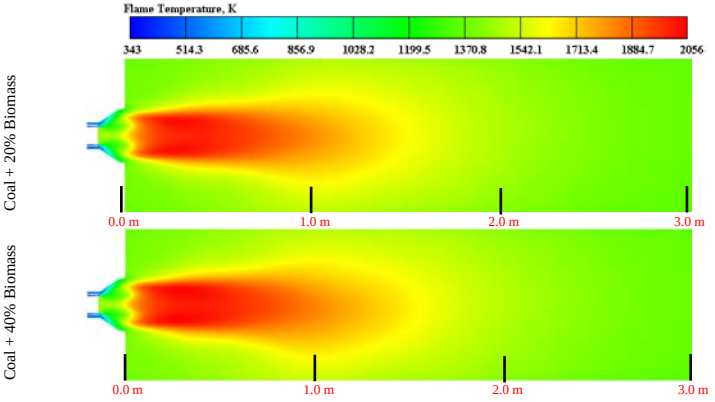

Figure 5: Flame temperature distribution on the horizontal plane for different Biomass sharing under oxy-firing (RR 75%) case.

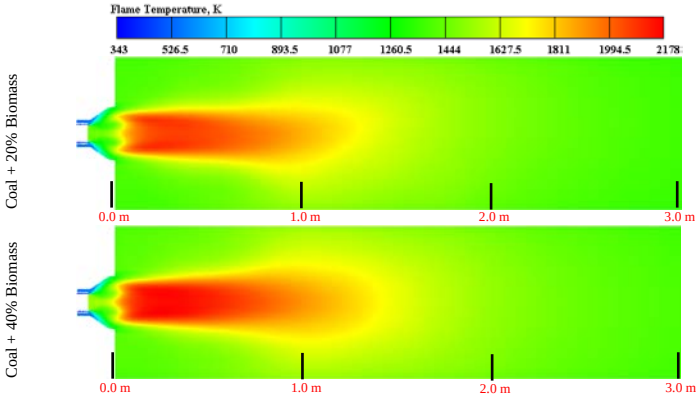

Figure 6: Flame temperature distribution on the horizontal plane for different Biomass sharing under oxy-firing (RR 72%) case.

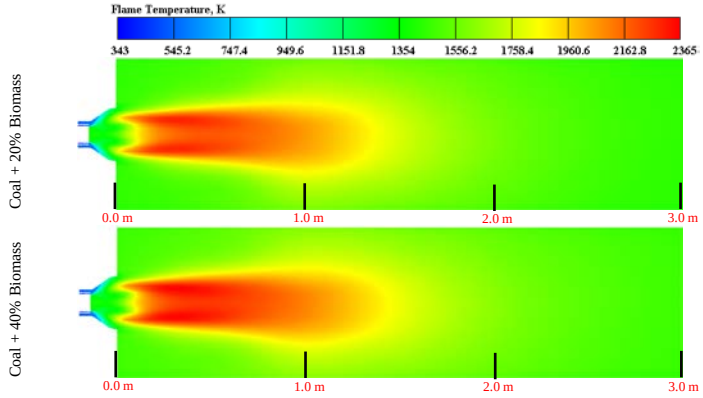

Figure 7: Flame temperature distribution on the horizontal plane for different Biomass sharing under oxy-firing (RR 68%) case.

Species mass fraction distribution for all the cases are presented in figure 8. Due to page limitations, results only for the 20% Biomass case are presented in this paper. Different species concentration such as (a).Carbon dioxide (CO_2), (b). Carbon monoxide (CO), (c). Hydrocarbon (CH_4), (d). Water vapour (H_2O) and (e). Hydrogen (H_2) mass fraction distributions are presented along the centre of the furnace from the exit of the burner under different combustion environment. Figure 10(a) represents the distributions of the CO_2 formation inside the furnace. From the figure it is found that for air firing case, CO_2 formation is below 20%. When transferred to oxy-firing cases, CO2 formation increases to 70-90% ranges. With the decrease of RR, maximum value of CO_2 is decreasing. Also, it is found in this study that with the increase of Biomass sharing, no significant changes for the formation of CO_2 is observed. So, it can be concluded that usage of Biomass is CO_2 neutral and fossil fuel can be totally replaced by the Biomass or partially replaced by increasing the Biomass sharing depending on the expected energy. In heterogeneous chemical process, CO is formed after the intermediate reaction of char with oxidizer which further produces emissions. CO distribution is shown in figure 8(b) for different cases. In this study, the hydrocarbon product from the devolatilisation is considered as equivalent to CH_4. Hydrocarbon (HC) mass fraction distribution is presented in Figure 10(c). When CO_2 concentration is low and O_2 concentration is high at RR68 case, peak of the HC is seen near the burner exit. With the increase of RR, HC mass fraction tends to zero. The formation of hydrogen (H_2) and water vapour (H_2O) mass fraction is related. With the decrease of RR, H_2 and H_2O both increase. While compared to air-firing case, increase in each mass fraction is found for all oxy-fuel cases. These are presented in figure 8(d) & (e) for H_2O and H_2 mass fraction distributions respectively. Prediction of Carbon in Ash (CIA) is an important achievement in this numerical study. Accurate prediction of CIA is a significant measure to determine the efficiency of Biomass co-combustion in a power plant. Figure 9 shows the comparison of numerical prediction and experimental measurement of Carbon-in-Ash (CIA). This prediction is only a qualitative measure. But overall, reasonable agreement has been observed between the numerical and the experimental data.

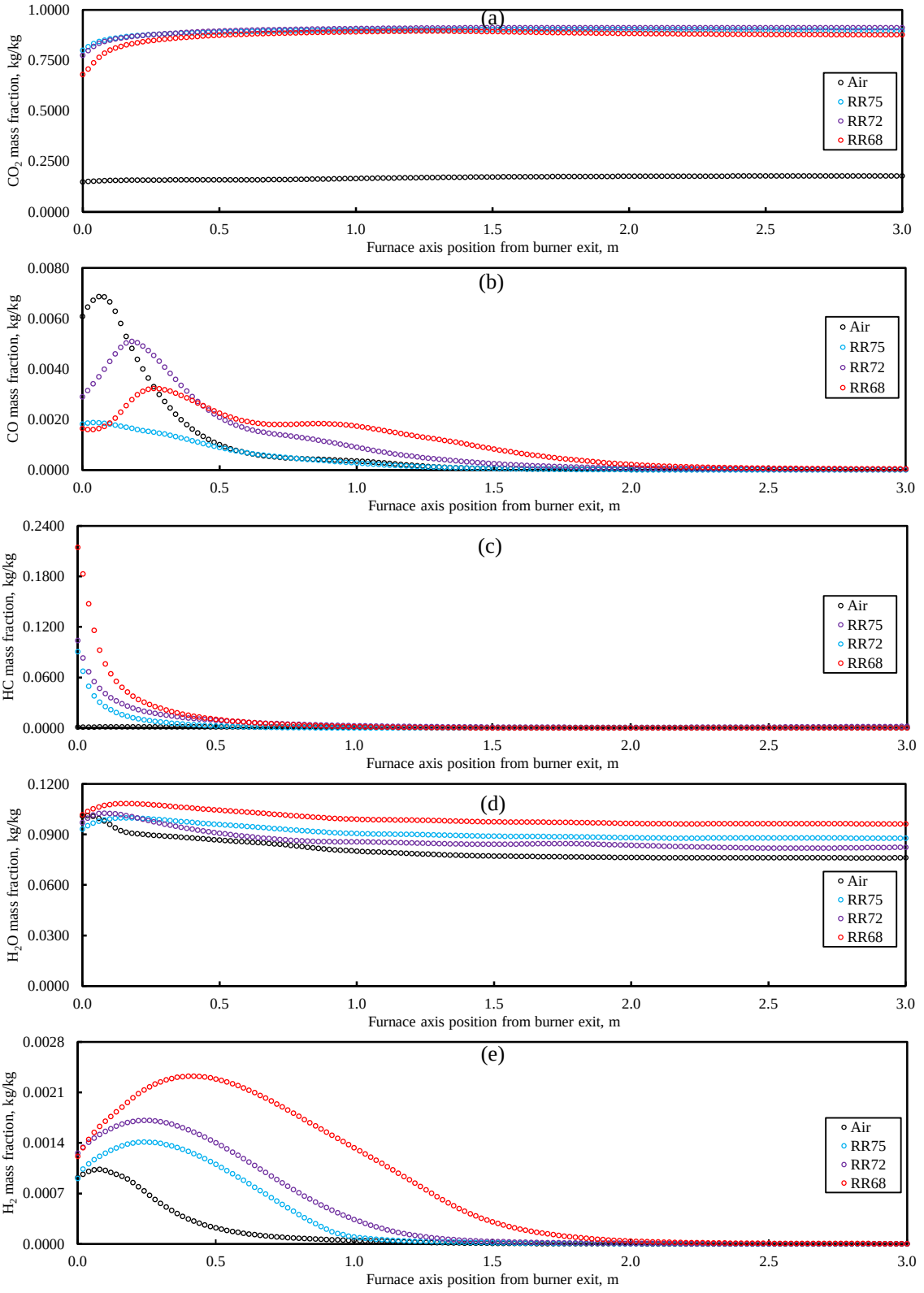

Figure 8: Species mass fraction distribution on axial direction for 20% Biomass sharing for different combustion environment.

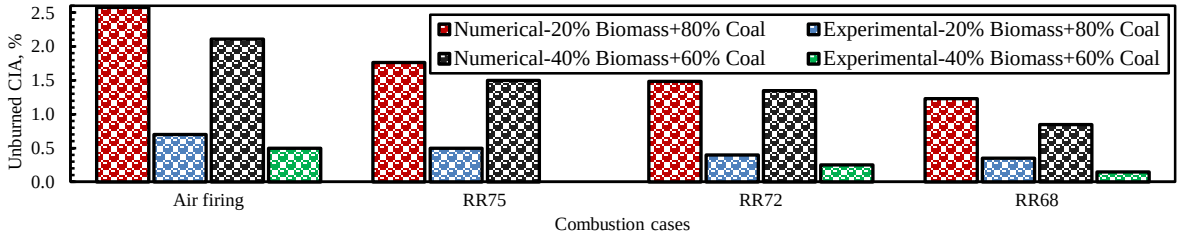

Figure 9: Comparison of numerical and experimental CIA measurement in different oxy-fuel co-firing conditions

Conclusion

Numerical modelling of Biomass co-combustion has been conducted considering Shea meal as a Biomass co-fired with Russian coal in a small scale furnace. In this study, different co-firing ratio such as 20% and 40% Biomass sharing has been investigated. A commercial CFD code coupled with some user defined program is incorporated to carry out the investigation. Grid sensitivity test has been conducted for a reference air firing case and the code was validated with the available experimental data. Results are presented for different combustion environment including air-firing and oxy-fuel combustion cases. The highlight of this study is to differentiate the effects of biomass sharing on the overall flame temperature. Also, related combustion species such as oxygen, carbon dioxide, carbon monoxide, hydrogen, water vapour, and hydrocarbon mass fraction distribution inside the furnace is identified. Furnace exit temperature and mean flame characteristics with the change of fuel ratio and flow condition has been studied. Finally, unburned Carbon in ash is predicted for all the cases and a reasonable agreement has been obtained.

Reference

1. Baxter, L., Biomass-coal co-combustion: opportunity for affordable renewable energy. Fuel, 2005. 84(10): p. 1295-1302.
2. Demirbas, A., Combustion characteristics of different biomass fuels. Progress in energy and combustion science, 2004. 30(2): p. 219-230.
3. Scheffknecht, G., et al., Oxy-fuel coal combustion—A review of the current state-of-the-art. International Journal of Greenhouse Gas Control, 2011. 5: p. S16-S35.
4. Haykiri-Acma, H., S. Yaman, and S. Kucukbayrak, Co-combustion of low rank coal/waste biomass blends using dry air or oxygen. Applied Thermal Engineering, 2013. 50(1): p. 251-259.
5. Sarabèr, A., Co-combustion and its impact on fly ash quality; pilot-scale experiments. Fuel Processing Technology, 2012. 104(0): p. 105-114.
6. Bragato, M., et al., Combustion of coal, bagasse and blends thereof: Part I: Emissions from batch combustion of fixed beds of fuels. Fuel, 2012. 96(0): p. 43-50.
7. Nussbaumer, T., Combustion and co-combustion of biomass: fundamentals, technologies, and primary measures for emission reduction. Energy & Fuels, 2003. 17(6): p. 1510-1521.
8. Smart, J.P., R. Patel, and G.S. Riley, Oxy-fuel combustion of coal and biomass, the effect on radiative and convective heat transfer and burnout. Combustion and Flame, 2010. 157(12): p. 2230-2240.
9. Smart, J.P., P. O'Nions, and G.S. Riley, Radiation and convective heat transfer, and burnout in oxy-coal combustion. Fuel, 2010. 89(9): p. 2468-2476.
10. Smart, J., et al., Characterisation of an oxy-coal flame through digital imaging. Combustion and Flame, 2010. 157(6): p. 1132-1139.
11. Bhuiyan, A.A. and J. Naser, Numerical modelling of oxy fuel combustion, the effect of radiative and convective heat transfer and burnout. Fuel, 2015. 139(0): p. 268-284.
12. Al-Abbas, A.H., J. Naser, and E.K. Hussein, Numerical simulation of brown coal combustion in a 550MW tangentially-fired furnace under different operating conditions. Fuel, 2013. 107: p. 688-698.
13. Al-Abbas, A.H., et al., Numerical Modelling of Oxy-Fuel Combustion in a Full-Scale Tangentially-Fired Pulverised Coal Boiler. Procedia Engineering, 2013. 56: p. 375-380.
14. Al-Abbas, A.H., J. Hart, and J. Naser, Numerical investigation of pyrolysis of a Loy Yang coal in a lab-scale furnace at elevated pressures. Heat and Mass Transfer, 2013. 49(12): p. 1725-1732.
15. Al-Abbas, A.H., J. Naser, and D. Dodds, CFD modelling of air-fired and oxy-fuel combustion in a large-scale furnace at Loy Yang A brown coal power station. Fuel, 2012. 102: p. 646-665.
16. Al-Abbas, A.H. and J. Naser, Effect of chemical reaction mechanisms and NO x modeling on air-fired and oxy-fuel combustion of lignite in a 100-kW furnace. Energy & Fuels, 2012. 26(6): p. 3329-3348.
17. Al-Abbas, A.H., J. Naser, and D. Dodds, CFD modelling of air-fired and oxy-fuel combustion of lignite in a 100KW furnace. Fuel, 2011. 90(5): p. 1778-1795.
18. Haider, A. and O. Levenspiel, Drag coefficient and terminal velocity of spherical and nonspherical particles. Powder Technology, 1989. 58(1): p. 63-70.
19. Spalding, D.B., Mixing and chemical reaction in steady confined turbulent flames. Symposium (International) on Combustion, 1971. 13(1): p. 649-657.

Available online at www.sciencedirect.com

ScienceDirect

Procedia Engineering 00 (2015) 000–000

Procedia Engineering

www.elsevier.com/locate/procedia

6th BSME International Conference on Thermal Engineering (ICTE 2014)

Modeling of slagging in industrial furnace: a comprehensive review

Arafat A. Bhuiyan and Jamal Naser*

Faculty of Science, Engineering and Technology (FSET)
Swinburne University of Technology, VIC-3122, Australia

Abstract

Slagging is a significant phenomenon related to ash handling and discharge in coal based power generation industries. The slag generally forms at high temperature on radiative refractory lined wall of the boiler. The progression of slagging arises over an extensive range of flue gas and surface temperatures and is dependent both on the characteristics of the ash and on the related design and operation conditions of the combustor. Proper understanding of the fundamentals of slagging is an important step for improvement of furnace design and ash related issues. Literatures review indicates insufficient progress in experimental as well as numerical context. Modeling may provide detailed investigations overcoming the limitation in experiment. This paper presents a short overview of the existing models and tools developed for the prediction of slagging behavior of the fuel ash in combustion applications. This article provides an extensive review of the fundamental aspects and emerging trends in numerical modeling of slag formation in industrial furnace. The attempts in modeling published so far are reviewed, grouped and summarized which will guide the researchers to further investigations.

Peer-review under responsibility of organizing committee of the 6th BSME International Conference on Thermal Engineering (ICTE 2014).

Keywords: CFD, Coal combustion, Slagging, Fouling, Webber number, Slag thickness, Combustor, Ash handling.

1. Introduction

Coal is the main fossil fuel energy sources in the world. It contains various inorganic contents such as SiO_2, TiO_2, Al_2O_3, CaO, MgO, Na_2O, K_2O, P_2O_5, Mn_3O_4, SO_3, Fe_2O_3 etc. During combustion of coal in power plant, these mineral contents are deposited as slag[1]. Slagging is a process of combustion in which ash component is

* Corresponding author. Tel.: +61 3 9214 8655; fax: +61 3 9214 8264.
E-mail address: jnaser@swin.edu.au

1877-7058
Peer-review under responsibility of organizing committee of the 6th BSME International Conference on Thermal Engineering (ICTE 2014).

heated (at a temperature above the ash fusion temperature) becomes molten and thus deposited along the furnace refractory wall. These molten ash forms a layer called slag. Fig. 1 demonstrates a typical slag layer formed in a 5MW combustion test facility [2]. The deposited slag thickness is not uniform in the ceiling wall (a) and the bottom wall (b) of the furnace. This slag layer has significant effect on performance of coal based furnace. The advantage of slagging is the reduction of the disposing of unused mineral content in the environment, energy efficiency, broader fuel flexibility, higher percentage of lower-carbon content slag residues for application [3, 4]. The deposited slag layer also works as a coating which prevents the heat loss in the gasifiers. But slagging reduces the overall efficiency of the furnace; excessive slagging reduces the reliability and safety because of corrosion. In order to maintain an optimum condition of slagging, a detailed fundamental of the slagging is important. For designing and optimization of slagging combustor, it is imperative to investigate the related process occurring inside the furnace. In last decade, research concentration has been given into the effects of oxy-fuel combustion by CFD [5-8]. But, limited attempts are taken to investigate the slagging issue. It is very important to know the amount and location of the slag as well as its dynamics. It is not possible to investigate the problems on site unobtrusively and with reasonable effort. The answer is numerical simulation which leads to slagging modeling. In recent years, a number of attempts have been made to utilize CFD methods to model the ash formation and transport process in pulverized fuel combustion system. Computational modeling is a way to investigate the performance of slagging for better understanding of this process. Modeling may provide detailed investigations overcoming the limitation in experiment.

The main objective of this study is to explore the fundamentals of slag flow modeling as limited progress in this issue is documented. This paper presents a short overview of the existing models and tools developed for the prediction of slagging behavior of the fuel ash in combustion applications. Overall, this paper provides an extensive review of the fundamental aspects and emerging trends in numerical modeling of slag formation in industrial furnace. The attempts in modeling published so far are reviewed, grouped and summarized which will guide the researchers to further investigations.

(a) (b)

Figure 1: The slag formed in the 5 MWth oxy-coal combustor [2], (a). at ceiling wall, (b). at bottom wall

2. Basics of slagging

The basic schematic illustration of the slag formation on a typical refractory wall and membrane wall are presented in figure 2. This figure illustrates the fundamentals of slag layer formation and associated mass and heat transfer processes. When molten ash particles hit the refractory wall, based on the capturing criteria, these particles are captured and deposited on the wall. Due to particle motion and the gravity effect, this newly formed molten slag layer are driven in the downwards direction. If the operating temperature is below the ash fusion temperature, a solid slag layer may be formed in between the molten slag layer and the wall. When the molten slag starts to solidify, its temperature is gradually decreased. [The nomenclature used in fig.2 are: T_{pt}=Slag phase transformation temperature which is also called temperature at critical viscosity, m_{in}= Ash particle hitting the slag layer, T_{in}= Ash particle temperature hitting the slag layer, T_{rs}=Temperature at solid slag and wall phase, T_{ts}= Temperature at refractory and steel wall, q_{in}= Syngas heat flux, δ_l= liquid slag thickness, δ_s=solid slag thickness, δ_t= total slag thickness, $m_{s,i}$=slag mass, $m_{ex,i-1}$=incoming slag mass flow rate, $m_{ex,i}$=Discharging slag mass flow rate, $q_{ex,i}$= discharging slag heat flux, $q_{ex,i-1}$=incoming slag heat flux and q_{out}= heat flux at wall.

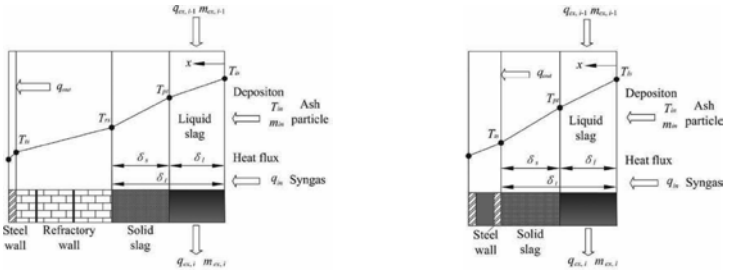

(a) (b)

Figure 2: Fundamentals of the slagging on the wall in gasifier (a, refractory wall; b, membrane wall) [9]

3. Methodology/modelling of slagging

In general, the modeling of slagging consists of several complexes and simultaneous processes such as the slag flow, particle capture and particle consumption modeling. Proper understanding and fundamentals in modeling of slagging is important. A graphical representation of the process involved in slag formation is given in figure 3. When the fuel particle hits the wall of the furnace, some of the particles are captured and some of the particles are rebound from the wall. The captured particles are passing through wall burning process [10]. As input conditions for the slag model, the heat fluxes, slag mass flow rates and gas temperatures can be integrated from the coupled CFD code. Seggiani [11], in his 1D modeling, illustrates an input-output variables scheme of the slag model coupled with 3D CFD code as shown in figure 4.

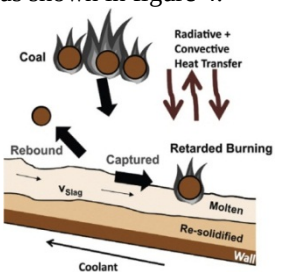

Figure 3: Process involved in slagging [10].

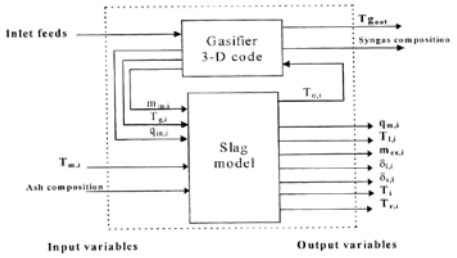

Figure 4: Parameters used in the integrated slag flow models [11]

3.1. Slag flow model

The slag flow model works based on Eulerian-Lagrangian approach which can be described by the mass, momentum and energy conservation equation as [10, 12]. In modeling of slag layer in solid fuel gasification process in [12], the significant assumptions considered as lower slag thickness, unidirectional flow, shear stress due to captured particles and slag properties are calculated at slag mean temperature. For the slag flow, Chen [2, 13] describes the 3 dimensional modeling that includes discrete phase and volume of fluid model for the modeling of slag layer in horizontal and vertical furnace respectively. Figure 5 shows an illustration of the mass momentum and energy balance in a finite volume (FV) of the slag layer. More details about these are documented in [2, 13].

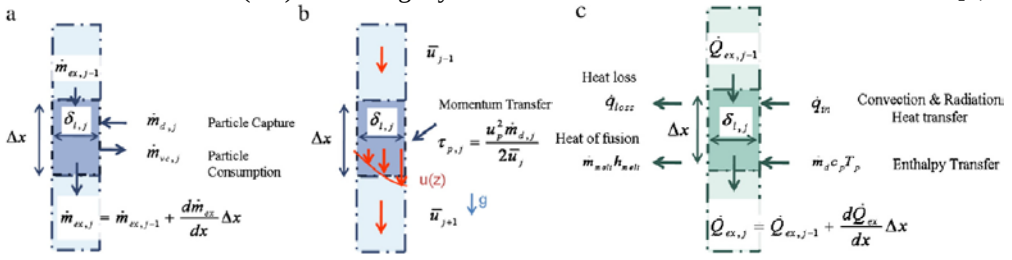

Figure 5: Representation of mass, momentum and energy balance of the liquid slag layer for vertical furnace [13]

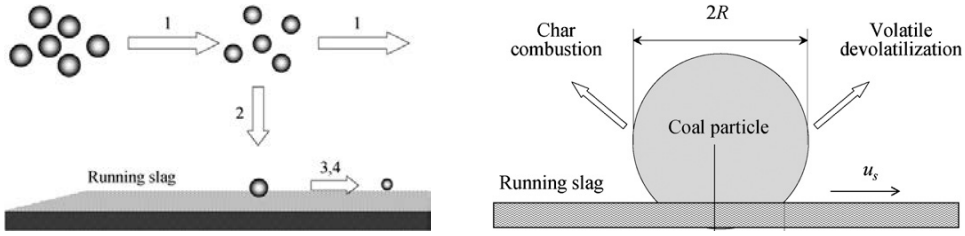

Figure 6: Diagram of (a). Particle burning in slagging combustor and (b). wall burning on running slag layer [14]

Table 1: Char capturing criteria used in [13]

Wall	Char/ash particle (T-Trap, R-Reflect)							
	$T_p > T_{cv}$				$T_p < T_{cv}$			
	Conversion > C_σ		Conversion < C_{cr} [15]		Conversion > C_{cr} [15]		Conversion < C_{cr} [15]	
	$We>We_{cr}$	$We<We_{cr}$	$We>We_{cr}$	$We<We_{cr}$	$We>We_{cr}$	$We<We_{cr}$	$We>We_{cr}$	$We<We_{cr}$
$T_{wi}<T_{cv}$	T	T	R	T	R	T	R	T
$T_{wi}<T_{cv}$	R	T	R	T	R	R	R	R

3.2. Char capture modeling

In coal combustion process, fuel particles are always at the state of melting. It is very difficult for them to drive back to spatial space. Particles having greater size try to be carried into the gaseous field again after depositing. In coal-fired boilers, the size of most particles is >1 mm, so most of the particles cannot go back to flow space. When these char/ash particles hit the furnace wall, most of the particles are captured on the wall and some particles are rebound from the wall. Determining the capturing/rebounding criteria is important in modeling the slagging in CFD. Several authors used particle capture sub model to define particle capturing criteria to form slag or not on the refractory wall. Chen [2, 13] developed the particle capture criterion considering three major parameters such as temperature of the particle, temperature of the combustor wall and the carbon conversion of the particle. Based on the assumptions [15, 16], when both the walls and the particles are sticky, the ash/char particle will be captured. If any one of the wall is not sticky, there is still a possibility for particle trapping. This is determined by the Webber number which is defined as the ratio of particle kinetic energy to the surface tension energy. The critical value of Webber number is assumed as 1.0 [17]. When Webber number cross the critical value, the particle is rebound. Based on the stickiness and the Weber number of the particles, the char capture criteria is summarized in [13] as shown in Table 1. Though a number of capturing criteria is developed, still a comprehensive modeling for the ash particle capture is required.

3.3. Wall burning sub-models

In slagging furnace, the process of free flow particle combustion, its depositions (trapping/rebounding) and wall burning are simultaneous process. These processes are interrelated and communicate with each other in terms of physical parameters like viscosity and temperature. The burning characteristics of particle on the molten slag layer with the associated process are presented in figure 6. Fundamentals about the wall burning process are given in [14, 18]. After, a char/ash particle is trapped on the refractory wall, is passes through the wall burning process starts. After sticking on the wall, the molten slag moves in the flow direction. Wall burning is a slower char combustion process because of the slower diffusion of oxygen on the particles external surface. To consider for the slower reaction of submerged particles in the wall slag layer, a wall burning sub model is proposed in [2, 10, 12, 13] which considers the sink position of the trapped particles.

3.4. Slag properties

Determination of slag properties such as viscosity, density, specific heat and thermal conductivity are dependent on ash composition, availability of oxygen and temperature [12]. The chemical compositions of the slag vary due to variation of coal slag origination. The slag mineral composition is usually measured by the use of X-ray

fluorescence (XRF) method. The temperature of critical viscosity is the most important property for slag modeling. The temperature of critical viscosity is a property which is challenging to predict which defines the liquid and solid slag layers interface. Due to lack of data from the experimental studies on the ash properties, sometimes properties are predicted based on correlations. The value of temperature at critical viscosity is suggested as 1680K in the correlations [11]. Determination of wall emissivity is another important factor. In the study of Ref [19], the slag emissivity having value of 0.83 were shown over the temperature range.

4. Recent numerical works

In recent years emphasis has been given on the furnace slagging problem as it is considered as a threat to the long term performance of the boiler. Many efforts have been given to identify the problems and related issues to avoid these problems experimentally. Several numerical studies were also carried out to investigate the fundamentals and detailed associated phenomenon in this problems. Table 2 shows the summarized endeavors in modeling the formation of slag by the researchers. Li [16, 20] conducted an experimental study to determine the physical phenomena associated with char–slag transition in an entrained-flow reactor. The physical properties of the char and slag particles were characterized, including the particle density, size, internal surface area and morphology. The major phenomena which indicate the char–slag transition are density increase, size reduction and surface area decrease. Predicted results showed that the particle capture efficiency was a function of coal conversion.

Seggiani [11] developed a simplified model for the simulation of time varying slag flow in a Prenflo entrained flow reactor of the IGCC Power plant, Spain. The furnace was operated at 25 bar supplied with coal and limestone mixtures as fuel. In modeling the slag formation, physical properties such as critical viscosity, specific heat, thermal conductivity are taken in to account. In this modeling, the gasifier wall was divided into 15 cells. This one dimensional slag building model can be described by the mass, momentum and energy quantity equation written for each control volume considering Reid and Cohen model assumptions [21]. This model is integrated with a 3D code to obtain mass deposition rate, gas temperature and heat flux. Figure 4 shows the implemented Input–output variables scheme of the integrated models in this code. The deposited slag thickness, temperature and heat flux were determined by using this model. Temperature of critical viscosity is considered as an important parameter which is dependent on the composition of slag. Wang [14, 18] developed a 1D steady state model to determine the deposition and burning characteristics during slagging co-firing of coal and wood. In this model, particle deposition, wall burning and slag flow are considered. Particle impingement and particle sticking characteristics are applied by using Wood's [22] and Walsh's [23] mechanisms. Particle stickiness dependent on critical temperature of ash particle which can be expressed in terms of slag softening temperature. The specialty of this model is the wall burning and slag flow process, but only limited for molten slag modeling. Compared to Seggiani's model, this typical model reflects the wall burning phenomenon when fuel particles are stuck on the slag surface and its consequence on char oxidation and heat transfer performance. But both of the model cannot determine the slag behavior in others direction. Yong [10, 12] developed a steady state model to describe the flow and heat transfer characteristics in slag layer of solid fuel gasifications by combining the model developed by Seggaini [11] and Wang [14, 18] as described earlier. In this modeling an updated temperature profile is assumed replacing Seggaini's assumptions.

Bockelie et al. [24] and Chen et al. [13]extended the 1D slag model into the 2D wall surface in fuel combustor. But slag flow is considered in one direction only. This 2D method considers the spatial distribution of ash particle deposition. This approach cannot completely solve the 3D flow behavior. Liu and Hao [25] modeled a two dimensional slag flow in an entrained flow gasifier using the Volume-of-Fluid (VOF) model. Ni et al. [9] used the same technique to model the multiphase multilayer slag flow and phase transformation considering two-dimensional mesh with uniform ash deposition rate.

Chen [2] developed a comprehensive 3D slag flow model to determine the slag behavior during coal combustion and gasification in a 5MW pressurized coal water slurry (CWS) vertically oriented oxy-fuel furnace. The model couples Volume of Fluid and Discrete Phase Model implemented in a commercial CFD code FLUENT using a detailed particle capture and wall burning sub model written and integrated with the CFD framework. This model fully resolves the three-dimensional characteristics of char/ash deposition, slag flow, as well as heat transfer through the slag layer. It was observed that molten ash properties are critical to the slag layer buildup.

Table 2: Summary of the modeling attempts for slagging

Simulated object		Modelling approach			Authors
Facility	Fuel	Code	Feature	Outcome/Limitations	
Prenflo gasifier IGCC power plant	Coal & Lime stone		One dimensional	This model provides the slag deposit thickness, the temperature across the deposit and heat flux to the metal wall. But this model cannot resolve the slag behaviour in the azimuthal direction.	Seggiani [11]
Pilot scale combustor	Coal & wood	WBSFPCC2	One dimensional steady state	This model demonstrates the deposition and burning characteristics during slagging co-firing, especially the wall burning mechanisms.	Wang [14]
Pilot scale combustor	Coal	WBSFPCC2	One dimensional steady state	This model considers wall burning sub process when particle are trapped on slag layer and its effects on the boiler wall performance. This model considers only molten slag thickness; no solid layer thickness is solved.	Wang [18]
Entrained flow gasifier	Chinese, Beisu and Boadian coal	FLUENT	Two dimensional Steady state	Developed a multiphase multilayer phase transformation model. The viscosity-temperature relationship in the liquid slag layer is established.	Ni [9]
5MWth ITEA Spa & ENEL combustor	Bituminous coal	FLUENT	Three dimensional Steady state	The accumulated molten slag is 1-2 mm having average slag velocity of 0.1mm.s due to high viscosity	Chen [2]
5MWth ITEA Spa & ENEL combustor	Bituminous coal	FLUENT	Two dimensional Steady state	Ash capturing ratio decreases with the increase of temperature of critical viscosity.	Chen [13]
5MWth ITEA Spa & ENEL combustor	Bituminous coal	FLUENT	One dimensional Steady state	It is found that wall traps about 56% of the coal particles fed in to the combustor. This model cannot resolve the slag behaviour in the azimuthal direction.	Yong [10, 12]
IGCC Power plant combustor	Coal, petcoke, waste	GLACIER	Two dimensional Steady state	This model has been demonstrated for oxygen blown, pressurized system, but for air blown or atmospheric system is not explored.	Bockelie [26]
High purity alumina reactor (T=1350°C)	SS001 coal, Funao-Sekiyama limestone	FLUENT	Steady state	A simple model was suggested for char capture by molten slag surface under high-temperature conditions.	Shimizu [27]
A lab-scale LEFR	Illinois 6 coal	FLUENT		Determines particle depositions behaviour during char slag transitions and established a criterion for accurately predicting particle fates.	Li [16]
Entrained-flow gasifier			One dimensional steady state	Slagging model has been developed based on the conceptual framework of carbon particle segregation.	Montagnaro [28]
FPTF at ABB	Wyoming and Oklahoma coal	PCGC-2	One dimensional Steady state	It was observed that heat flux and the deposition rate had a substantial effect on the thermal and physical properties.	Richards [15]
512-MW boiler at	EERC's coal	AshProSM		It assesses the combined impact of ash formation and deposition phenomena, fuel quality, ash properties, slagging.	Ma [29]

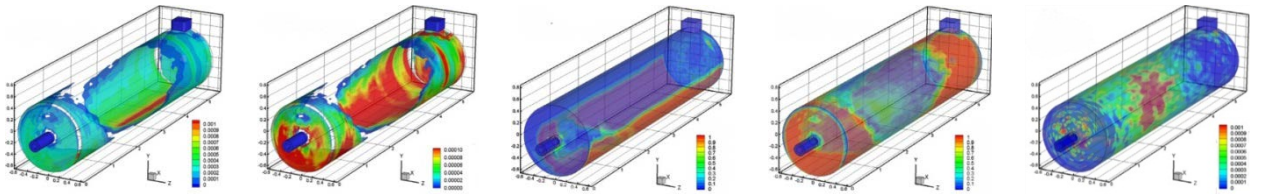

(a) (b) (c) (d) (e)

Figure 7. 3D simulated results in a 5MW combustion test facility [at t= 5.8 h]; (a) Molten slag thickness (mm), (b) The slag surface flow velocity (m/s), slag volume fraction near the wall, (c) without & (d) with particle dispersion model and (e) slag deposition rate (kg/m^{2}s) [2]

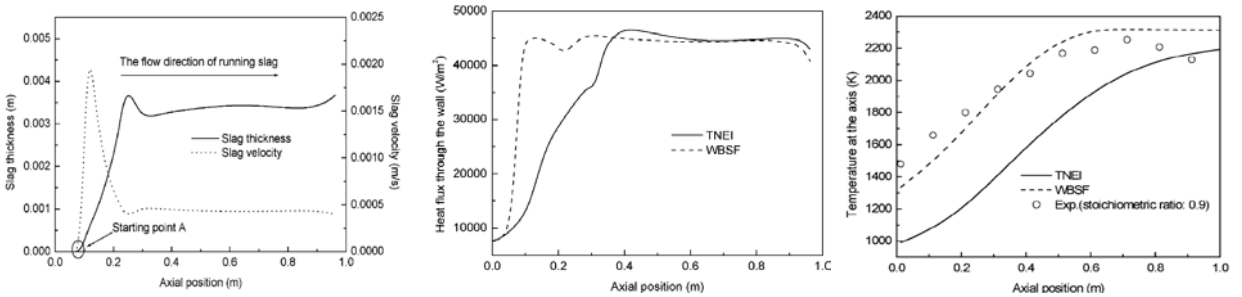

(a) (b) (c)

Figure 8: (a). Relationship between slag thickness and slag velocity in axial direction of the furnace [14], (b). Heat flux distribution through the slag layer and refractory wall along the axial distance [14] & (c). Temperature distributions in the slag layer as a function of axial distance [14].

Chen [2] developed a comprehensive three dimensional slag flow model to determine the slag behavior during coal combustion and gasification in a 5MW pressurized coal water slurry (CWS) vertically oriented oxy-fuel furnace. The model integrated different models for fluid and particle trajectories modeling implemented in a commercial CFD code FLUENT using a detailed particle capture and wall burning sub model written and integrated with the CFD framework. The VOF model was used for slag flow modeling and the Discrete Phase Model (DPM) was used for fuel particle trajectories modeling. This model completely decides the 3D features of char/ash deposition, slag flow, as well as heat transfer through the slag layer. Effect of temperature at critical viscosity and viscosity of slag formed are important in the process of slagging (both molten and solid slag). The proportion of ash captured on the cylindrical wall decreases when temperature at critical viscosity increases. The slag thickness, velocity, and heat transfer were predicted for both the furnaces.

Figure 7 shows the visualization of the molten slag thickness, slag surface flow velocity, slag volume fraction near the wall respectively based on [2]. The result showed that 1–2 mm slag layer is formed on the refractory wall which is basically molten. These molten slags runs downward on the refractory wall, gathers on the floor of the furnace and exits at the lower wall of the combustor, mostly driven by gravity for the horizontal furnace. The mean slag flow rate is normally about 0.1 mm/s. Overall, this three dimensional model is general enough to predict the coal slagging gasification and burning of coal with other combustor designs. In all the furnaces, near the inlet region, both the velocity and slag thickness are very small for comparatively lower temperature. When the temperature crosses the melting point temperature, slags are appeared. The relationship between the slag thickness and slag velocity, heat flux and slag temperature are presented in figure 8 based on the numerical work of [14]. It is observed that slag velocity decreases with the increase of slag thickness. Similar trends is observed in the study of [2].

5. Conclusion

Slagging is termed as a disease in combustion equipment. Understanding of the fundamentals of slag formation is an important phase for development of boiler design and ash related issues. This paper demonstrate a comprehensive review of the slag formation behavior and related process involved during slagging combustion in coal based power plant. Literature shows few attempts addressing this issue. Computational modeling is a possible way to investigate

the formation and transportation process involved in slag formation. Most of the numerical attempts are limited to one or two dimensional which cannot predict the slagging behavior precisely. This article offers an extensive review of the fundamental aspects and emerging trends in numerical modeling of slag formation in industrial furnace. The attempts in modeling published so far are reviewed, grouped and summarized. Also, slag flow model, char capturing criteria, wall burning model are described in details. Overall, this study will provide a guideline to the researchers for further investigation.

References

1. Wall, T., et al., Coal ash fusion temperatures—new characterization techniques, and implications for slagging and fouling. Progress in energy and combustion science, 1998. 24(4): p. 345-353.
2. Chen, L. and A.F. Ghoniem, Development of a three-dimensional computational slag flow model for coal combustion and gasification. Fuel, 2013. 113: p. 357-366.
3. Beér, J.M., Combustion technology developments in power generation in response to environmental challenges. Progress in Energy and Combustion Science, 2000. 26(4): p. 301-327.
4. Fen, J., Principles and Calculations of Boilers. 2nd edition. Science Press, Beijing, 1992.
5. Bhuiyan, A.A. and J. Naser, Computational modelling of co-combustion of coal and biomass under oxy-fuel condition in a small scale furnace. Fuel, In press.
6. Bhuiyan, A.A. and J. Naser, Numerical modelling of oxy fuel combustion, the effect of radiative and convective heat transfer and burnout. Fuel, 2015. 139(0): p. 268-284.
7. Al-Abbas, A.H., J. Naser, and D. Dodds, CFD modelling of air-fired and oxy-fuel combustion in a large-scale furnace at Loy Yang A brown coal power station. Fuel, 2012. 102: p. 646-665.
8. Al-Abbas, A.H. and J. Naser, Effect of chemical reaction mechanisms and NO x modeling on air-fired and oxy-fuel combustion of lignite in a 100-kW furnace. Energy & Fuels, 2012. 26(6): p. 3329-3348.
9. Ni, J., et al., Molten slag flow and phase transformation behaviors in a slagging entrained-flow coal gasifier. Industrial & Engineering Chemistry Research, 2010. 49(23): p. 12302-12310.
10. Yong, S.Z. and A. Ghoniem, Modeling the slag layer in solid fuel gasification and combustion–Two-way coupling with CFD. Fuel, 2012. 97: p. 457-466.
11. Seggiani, M., Modelling and simulation of time varying slag flow in a Prenflo entrained-flow gasifier. Fuel, 1998. 77(14): p. 1611-1621.
12. Yong, S.Z., M. Gazzino, and A. Ghoniem, Modeling the slag layer in solid fuel gasification and combustion–Formulation and sensitivity analysis. Fuel, 2012. 92(1): p. 162-170.
13. Chen, L., S.Z. Yong, and A.F. Ghoniem, Modeling the slag behavior in three dimensional CFD simulation of a vertically-oriented oxy-coal combustor. Fuel Processing Technology, 2013. 112: p. 106-117.
14. Wang, X., et al., Modeling of a coal-fired slagging combustor: Development of a slag submodel. Combustion and Flame, 2007. 149(3): p. 249-260.
15. Richards, G.H., P.N. Slater, and J.N. Harb, Simulation of ash deposit growth in a pulverized coal-fired pilot scale reactor. Energy & Fuels, 1993. 7(6): p. 774-781.
16. Li, S., Y. Wu, and K.J. Whitty, Ash deposition behavior during char− slag transition under simulated gasification conditions. Energy & Fuels, 2010. 24(3): p. 1868-1876.
17. Senda, J., et al., Modeling of diesel spray impinging on flat wall. JSME international journal. Series B, fluids and thermal engineering, 1996. 39(4): p. 859-866.
18. Wang, X., et al., The deposition and burning characteristics during slagging co-firing coal and wood: modeling and numerical simulation. Combustion Science and Technology, 2009. 181(5): p. 710-728.
19. Mills, K.C. and J.M. Rhine, The measurement and estimation of the physical properties of slags formed during coal gasification: 1. Properties relevant to fluid flow. Fuel, 1989. 68(2): p. 193-200.
20. Li, S. and K.J. Whitty, Physical phenomena of char–slag transition in pulverized coal gasification. Fuel Processing Technology, 2012. 95: p. 127-136.
21. Reid, W. and P. Cohen, Factors affecting the thickness of coal-ash slag on furnace-wall tubes. Trans. ASME, 1944. 66: p. 685-690.
22. Wood, N., Mass Transfer of Particles and Acid Vapor to Cooled Surfaces. Journal of the Institute of Energy, 1981. 54(419): p. 76-93.
23. Walsh, P.M., A.F. Sarofim, and J.M. Beer, Fouling of convection heat exchangers by lignitic coal ash. Energy & fuels, 1992. 6(6): p. 709-715.
24. Bockelie, M., et al., CFD modeling for entrained flow gasifiers in Vision 21 Systems, 2003.
25. Liu, S. and Y. Hao. Numerical study on slag flow in an entrained-flow gasifier. in ASME 2007 International Mechanical Engineering Congress and Exposition. 2007. American Society of Mechanical Engineers.
26. Bockelie, M.J., et al., CFD modeling for entrained flow gasifiers. 2002.
27. Shimizu, T. and H. Tominaga, A model of char capture by molten slag surface under high-temperature gasification conditions. Fuel, 2006. 85(2): p. 170-178.
28. Montagnaro, F. and P. Salatino, Analysis of char–slag interaction and near-wall particle segregation in entrained-flow gasification of coal. Combustion and Flame, 2010. 157(5): p. 874-883.
29. Ma, Z., et al., A comprehensive slagging and fouling prediction tool for coal-fired boilers and its validation/application. Fuel Processing Technology, 2007. 88(11): p. 1035-1043.

Available online at www.sciencedirect.com

ScienceDirect

Procedia Engineering 00 (2015) 000–000

Procedia Engineering

www.elsevier.com/locate/procedia

6th BSME International Conference on Thermal Engineering (ICTE 2014)

Flameless "Cool" Combustion in Multi-phase Configuration

Tanvir Farouk*

Department of Mechanical Engineering, University of South Carolina, Columbia, South Carolina, 29208, USA

Abstract

Cool flames are commonly associated with engine-knock phenomenon in spark ignition engines and autoignition in diesel engines, and results from low temperature partial oxidation of the fuel air mixture that eventually leads to hot flame ignition. However, the possibility of a cool flame supporting quasi-steady combustion of a fuel droplet has never been speculated, let alone been experimentally observed. Recent microgravity droplet combustion onboard the International Space Station (ISS) under the Flame Extinguishment (FLEX) Experiment Program showed anomalous combustion of *n*-heptane droplets; high temperature combustion followed by radiative visible extinction and a transition to a second stage burn characterized by loss of visible flame emission. In the second stage the droplet regression continues eventually resulting in extinction diameters characteristic of diffusive extinction. Experimental examples of the two stage burning and extinction characteristics of isolated *n*-heptane droplets under microgravity conditions are presented and analyzed numerically. Predictions show that the second stage combustion occurs as a result of chemical kinetics associated with classical premixed "*Cool Flame*" phenomena. In contrast to the kinetic interactions responsible for premixed cool flame properties, those important to cool flame droplet burning are characteristically associated with the temperature range between the turnover temperature and the hot ignition. Initiation of and continuing second stage combustion involves a dynamic balance of heat generation from diffusively controlled chemical reaction and heat loss from radiation and diffusion. Within the noted temperature range, increasing reaction temperature leads to decreased chemical reaction rate and vice versa. As a result, changes of heat loss rate are dynamically balanced by heat release from chemical reaction rate as the droplet continue to burn and regress in size. Factors leading to initiation of the second stage burning phenomena are also investigated. The chemical kinetics dictating the second stage combustion and extinction process is also discussed.

Peer-review under responsibility of organizing committee of the 6th BSME International Conference on Thermal Engineering (ICTE 2014).

Keywords: Droplet Combustion; Multi-stage Combustion; "Cool" Flames

* Corresponding author. Tel.: +1-803-777-3380; fax: +1-803-777-0106.
E-mail address: tfarouk@sc.edu

Peer-review under responsibility of organizing committee of the 6th BSME International Conference on Thermal Engineering (ICTE 2014).

1. Introduction

Since 2009, the **Fl**ame **Ex**tinguishment (FLEX) Experiment has been conducting isolated droplet combustion experiments aboard the International Space Station (ISS). The overall goal of these experiments is to determine and analyze burning behavior, limiting oxygen index, and extinction mechanisms as a function of fuel, drop diameter, pressure, oxygen index, and dilution (using various diluents, including helium, nitrogen, and carbon dioxide) [1]. Unique to microgravity experiments is the ability to study a wide range of initial drop diameters so as to characterize both radiative and diffusive extinction phenomena. In the first phase of the program, methanol was utilized to obtain data on a non sooting fuel which absorbs combustion products over its burning history, notably water [1, 2]. More recently, the study of hydrocarbons was initiated using *n*-heptane as the fuel. In the case of methanol, classical diffusive and radiative extinction phenomena are observed, and a detailed numerical analysis of the results has recently appeared [2]. In the *n*-heptane experiments, radiative heat loss from larger diameter, ignited droplets results in cessation of classical (high temperature) droplet combustion behavior at a relatively large droplet size. In contrast to the classical radiative extinction observed with methanol, a transition to a second stage of low temperature constant burning rate behavior characterized by loss of visible flame emission follows; indicating an anomalous combustion characteristic. In this second stage the droplet continues to undergo rapid and apparent quasi-steady vaporization without the presence of a visible flame. This second stage burning and droplet regression continues, eventually resulting in diffusive extinction at a finite drop size that then apparently experiences additional time-dependent evaporation into the surrounding environment. This dual mode of combustion is only observed for sufficiently large initial droplet diameter; at smaller droplet diameters, classical single stage burning and high temperature diffusive extinction occurs.

Simulations are conducted to elucidate the influence of the coupled physico-chemical processes that triggers the observed dual-mode behavior. Simulations were conducted using a recently developed, one-dimensional, spherosymmetric, transient combustion model [3]. The predictions from the model is compared against the recent ISS *n*-heptane droplet experiments [1]. Predictions from the model were found to compare favorably with the experimentally measured droplet and flame diameter evolution. Special attention is given to delineate whether the observed flames result from classical NTC, *"Cool Flame"* kinetic behavior or are other driving factors responsible for the dual-mode/two stage combustion process.

2. Mathematical Model

The mathematical model employed in this current work is a transient, spherosymmetric droplet combustion model featuring detailed gas phase kinetics, spectrally resolved radiative heat transfer and multi-component gas phase transport. Details of the model have been reported in some of our recent publications [2, 4]. A brief description of the model is provided here. The model comprises of species conservation for each of species considered and energy conservation in both the phases. The complete set of coupled partial differential and algebraic equations are discretized first in space and then integrated in an automated fashion as a set of coupled ordinary differential-algebraic equations in time. Spatial discretization is performed according to a node-centered finite volume scheme with a second order accuracy. The volume boundaries are defined to coincide with the liquid–gas interfacial and the far field (two hundred times the initial droplet diameter) boundary is well defined using Dirichlet conditions and remains fixed in the simulations. The Dirichlet conditions imposed on the far-field are of fixed ambient composition and temperature. The innermost liquid node is centered at the origin, providing the required no-flux condition. The discretized mass flux is represented on cell interfaces and not cell centers, in the manner traditionally referred to as a staggered grid to avoid oscillatory solutions. Numerical integration of the final set of discretized equations is performed using a backward difference formula with a variable order of up to fifth order and a variable time step utilizing a fully implicit multipoint interpolation. This makes it appropriate for the large range of time scales and stability constraints imposed by chemically reacting systems when combined with automatic time-step variation.

3. Results and Discussion

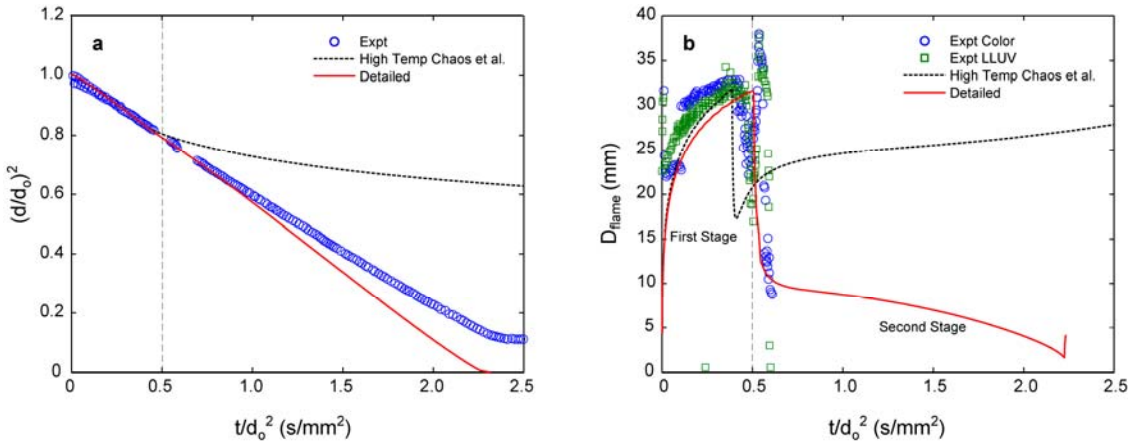

Fig. 1. Measured and predicted evolution of : (a) droplet diameter and (b) flame radius for a *n*-heptane droplet in ambient air (d_o = 3.91 mm, 0.21 X_{O2}, 0.79 X_{N2}, one atmosphere pressure). The experimental data are that of [1]. The flame radius experimental data contains measurement from both a color camera (Color) and low light UV (LLUV) camera. Predictions are shown with both the detail chemical kinetics model and the high temperature *n*-heptane model of Chaos et al. [5].

To get insight into the anomalous dual stage burning characteristics and hence affirm the combustion regime simulations were conducted with two chemical kinetics model, a "detailed" chemical kinetics model and a high temperature *n*-heptane chemical kinetic model [5] separately. It should be noted that the "high temperature" model of Chaos et al. was specifically developed for high temperature oxidation and did not include any low and intermediate temperature reaction pathways. Figure 1 shows the predicted droplet and flame diameter evolution from both these kinetic models and compares them to the experimental measurements [1]. The experimental conditions are d_o = 3.91 mm, 0.21 X_{O2}, 0.79 X_{N2}, one atmosphere pressure and is referred to as the base case. It can be seen that the predictions from the two kinetic models are distinctively different. The "high temperature" model predicts extinction of the droplet at a large droplet size due to radiative heat losses [2, 6] associated with the larger droplet size. After extinction the droplet is predicted to undergo evaporation in the quiescent environment, which is evident in the droplet diameter regression. Consistently the flame diameter evolution predictions with "high temperature" model shows an abrupt decrease corresponding to the flame extinction. In the simulations the peak temperature is utilized as the flame position marker as has been done some of our previous work. [2, 3]. As a consequence the flame diameter shows continuing evolution even after extinction. The "detailed" model shows significantly different combustion characteristics and captures the experimental observation qualitatively. The "detailed" model indicates that following the visible flame extinction which corresponds to the typical radiative extinction the droplet transitions to a second stage combustion where droplet diameter regresses at a significantly higher rate suggesting higher burning rate. In addition the "detailed" model predicts extinction towards the end of the second stage burn. During this second stage the flame diameter is found to be significantly smaller, locating itself very close to the droplet surface. Due to the large radiative heat loss (Figure 4) the flame positions itself closer to the droplet surface to compensate and sustain continuous burning. It can be seen that during the second stage the flame temperature is significantly lower and has a value of ~ 750K. The predictions from the "detailed" model are very similar to the "high temperature" model in the first stage the only difference being the temporal location of the transition. In comparison to the experiments the "high temperature" model shows an earlier extinction of the visible flame in contrast the "detailed" model predicts the transition to occur slightly later and is in good agreement with the experiments. Even though the "detailed" model qualitatively captures the experimental measurements, the second stage burning rate is significantly over predicted and vice versa for the extinction diameter. The predicted extinction diameter was found to be ~0.35 mm being smaller by a factor of 3.5 than the experiment.

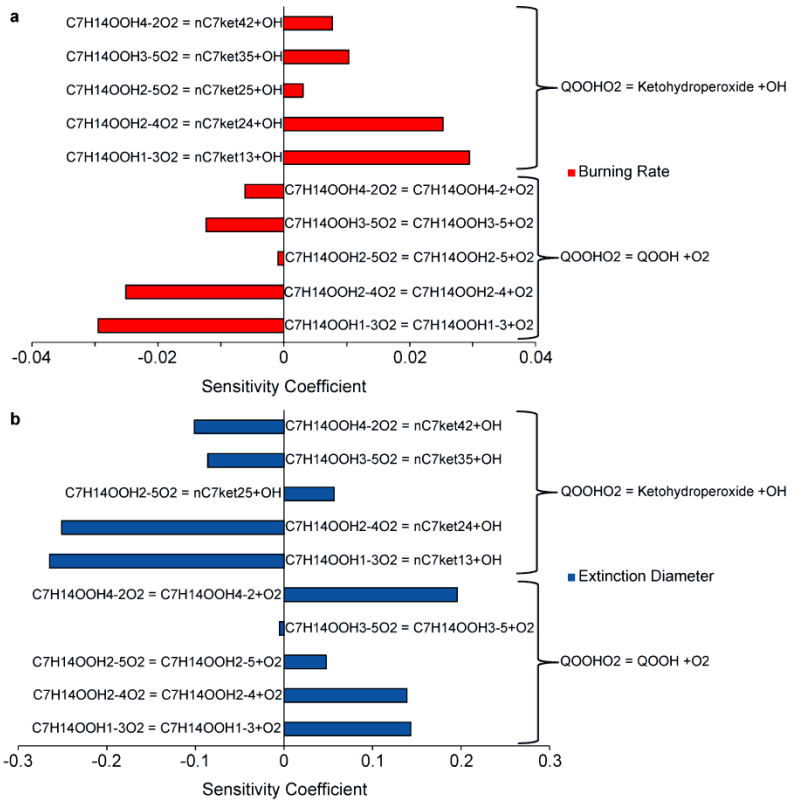

Fig. 2. Prominent sensitivity coefficients of (a) average burning rate $K_{b\,avg}$ and (b) extinction diameter d_{ext} on reaction rate coefficients (d_o = 3.91 mm, 0.21 X_{O2}, 0.79 X_{N2}, one atmosphere pressure).

The "detailed" model only provided qualitative agreement with the experimental measurement thus it is critical to obtain insight into the defining parameters of this discrepancy and at the same time determine the uncertainty limits of the predictions. The predictions from the "detailed" model showed very good agreement with the first stage measurement data. It is therefore the second stage combustion process that is not accurately predicted. As such simulations were conducted by perturbing each of the low temperature reactions individually (increase/decrease by a factor 2) to obtain the uncertainty bandwidth of the predictions and at the same time find out the sensitivity of the reactions to the average burning rate ($K_{b\,avg}$) and extinction diameter (d_{ext}). Figure 2 depicts the prominent sensitivity coefficients of droplet burning rate and extinction diameter on the reaction rates for the second stage burn. The sensitivity coefficient is identified as $S = \partial \log F(k) / \partial \log k = \partial F(k)\ k / \partial k\ F(k)$ where F is the target value which for this case is the average burning rate and extinction diameter. The sensitivity coefficient can be expressed by a finite difference formula, $S = [F(2k) - F(0.5k)]k / 1.5k\ F(k) = [F(2k) - F(0.5k)] / 1.5F(k)$, where the numerator represents the difference in the target value when the reaction rate is increased and decreased by a factor of two and the denominator denotes the target value for an unperturbed reaction rate. A positive sensitivity coefficient corresponds to a direct influence i.e. an increase in the parameter results in an increase in the target value and vice versa for negative sensitivity coefficient. The reactions having the most influence on the second stage burn was found to be isomerization of $QOOHO_2$ to ketohydroperoxide ($QOOHO_2 \rightarrow Ketohydroperoxide + OH$) and dissociation of $QOOHO_2$ ($QOOHO_2 \rightarrow QOOH + O_2$); Q = C_7H_{14} for this case. In general, increase in the rate of $QOOHO_2 \rightarrow Ketohydroperoxide + OH$ increased the burning and consequently decreased the extinction diameter. A vice versa is observed for the dissociation reactions. At temperatures lower than approximately 900K, the β-scission of alkyl radicals and internal H-atom abstraction reactions are slow to occur due to their high activation energies [7]. Under these conditions the most of the alkyl radicals (R) go through O_2 addition resulting in the formation of alkyl peroxy radicals RO_2. The alkyl peroxy radicals (RO_2) undergo isomerization to form QOOH which is the major pathway for the production of QOOH. The $QOOHO_2$ is formed by the addition of O_2 with

QOOH. At the low temperature regime the chain branching is mainly due to the reaction pathway leading through the ketohydroperoxide species. Hence the $QOOHO_2 \rightarrow Ketohydroperoxide + OH$ reactions have a positive effect on the second stage burning rate and vice versa for the extinction diameter. On the other hand the chain propagation reactions of QOOH species leads to the formation of cyclic ether, conjugate olefins and β decomposition products resulting in lower reactivity in the NTC regime. Therefore an increase in the $QOOHO_2$ dissociation rate to QOOH + O_2 decreases the second stage burning rate and accordingly increases the extinction diameter.

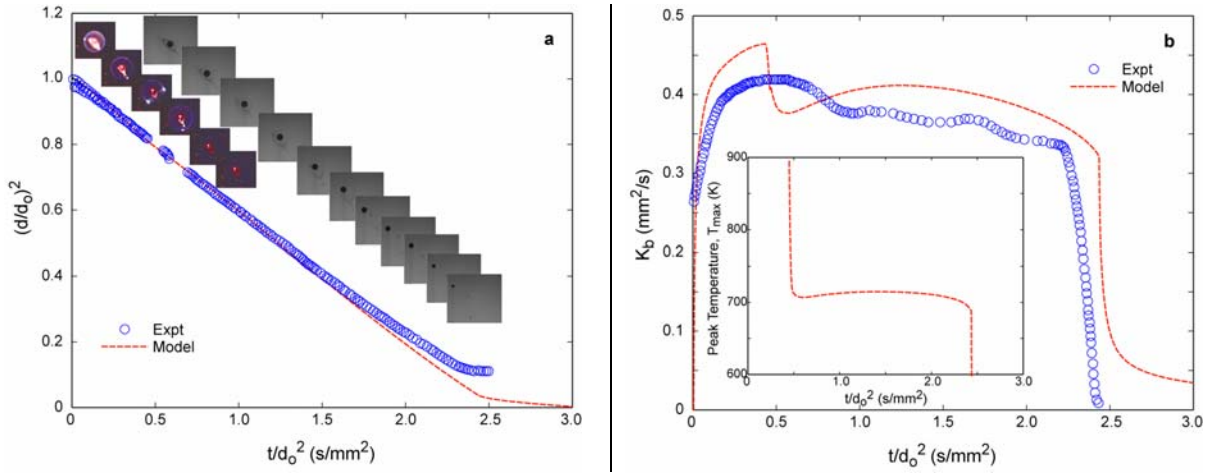

Fig. 3. Predicted evolution of (a) droplet diameter and (b) burning rate with the revised chemical kinetics model (d_o = 3.91 mm, 0.21 X_{O2}, 0.79 X_{N2}, one atmosphere pressure). Inset of experimental visualization of flame and droplet diameter is also provided which shows the continuing diameter regression after the flame extinguishment.

After identifying the most sensitive reactions for the second stage burn, simulations were conducted by modifying the reaction rates of these ten reactions to their uncertainty limit. For that the reaction rates for the $QOOHO_2 \rightarrow Ketohydroperoxide + OH$ reactions were decreased by a factor of 2 and the reaction rates for the $QOOHO_2 \rightarrow QOOH + O_2$ reactions were increased by a factor of 2. It should be noted though that the modification of these ten reaction rates is simply to observe their combined influence on the droplet combustion characteristics and it also brings forth the notion that the reaction rates for these ten reactions should be further investigated which is however not a scope of this work. Figure 3 presents the comparison of the measured and predicted droplet diameter and burning rate evolution utilizing the revised chemical kinetics model. It is evident that the predictions from the revised chemical kinetic model show better agreement with the measurements. The predicted average burning rate is obtained by time-averaging the instantaneous burning rate (K_o) between $t = 0.1t_b$ and $t = 0.95t_b$ where t_b is the total burn time (ignition to extinction). Comparing to the base kinetic model the revised chemical kinetics model predicts an average burning rate ($K_{b\,avg}$) of 0.385 mm^2/s and extinction diameter (d_{ext}) of 0.95 which is lower and higher by a factor of 1.15 and 2.38 respectively. In addition the second stage flame temperature is predicted to be~ 700 K by the revised kinetic model which is lower by 50 K than that of the base kinetic model predictions. However it should be noted that the model slightly over predicts the average burning rate and vice versa for the extinction diameter in comparison to the experimental measurements. The disparity between the two is most possibly a result of the well known perturbing effect of drift velocity. Ignition delay time and oxidation speciation predictions with the revised kinetic model were also found to be in improved agreement in the low and NTC temperature regime.

The integrated heat generation ($Q_{generation}$) and losses due to radiation ($Q_{radiation}$) and conduction ($Q_{conduction}$) are presented in Figure 4. Figure 4 shows that the integrated heat generation has a very sharp rise during ignition which also decreases very rapidly as a somewhat quasi-steady diffusion flame structure is established. The decrease in $Q_{generation}$ after ignition is also a consequence of the increasing radiative loss $Q_{radiation}$ during the first stage of the burn when the flame radius is still increasing (Figure 1). At the same time the conductive heat losses is also substantial. In this first stage of combustion the radiative heat loss is almost a factor of ~ 2 higher than the conductive losses. It can

be clearly seen that the transition to the second stage "*cool flame*" like behavior is initiated by the heat loss mechanism. The transition to the second stage occurs when the summation of the heat loss terms are close to the heat generation. As significant heat loss dominates the combustion process the flame positions itself close to the droplet surface for compensation as it is evident in Figure 3. During the second stage the $Q_{generation}$ is found to be ~ 17 W. On the basis of a time averaged heat generation rate of 150 W in the "high temperature" first stage the heat generation in the second stage is found to be ~ 11.5%. It is interesting to further note that during the second stage the dominant heat loss mechanism transforms to conduction from radiation. This is due to the fact that during the second stage as the flame is very close to the droplet surface the radiative heat loss decreases significantly.

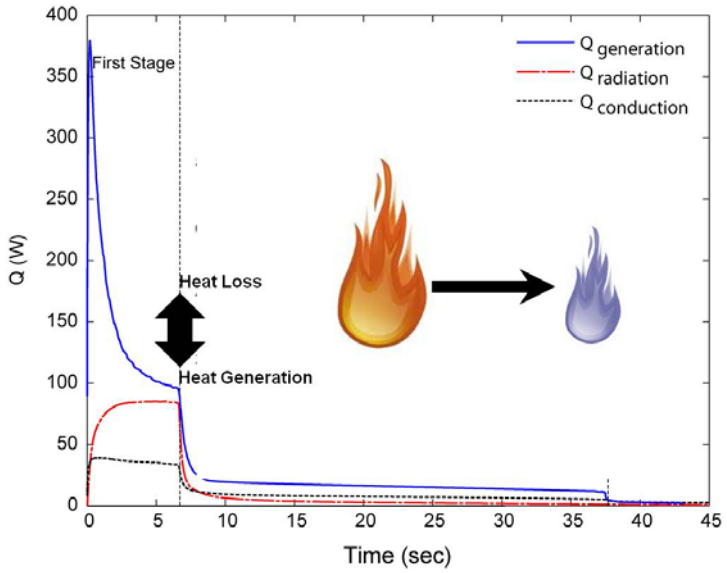

Fig. 4. Total heat generation, radiative and conductive heat losses for a *n*-heptane droplet undergoing two stage combustion in air (d_o = 3.91 mm, 0.21 X_{O2}, 0.79 X_{N2}, one atmosphere pressure).

More recent ISS *n*-heptane isolated droplet combustion experiments at three atmospheres pressure and the same oxygen index but with diluents inhibiting heat loss shows "multiple cycles" of dual stage combustion i.e. *hot – cool* flame transitions. The experiments are typically conducted for larger droplet sizes, d_o ~3 – 5 mm. For every experiment the combustion chamber is filled with the desired ambient gas mixture, consisting of oxygen, nitrogen and carbon dioxide to a pressure of 3.0 atm. In these experiments the flame steadily grows in diameter and decreases in luminous intensity to the point at which it reaches its maximum diameter where it then either suddenly extinguishes or begins to exhibit oscillatory behavior just prior to extinguishing. The oscillatory behavior is marked by repeated transitions between a complete and partial spherical flame surface and lasts for a brief period of time before completely extinguishing. The extinction of the visible flame commences the low temperature second stage burning regime, qualitatively referred to as the "*Cool Flame*" regime. During the second stage burning, rapid droplet vaporization persists and is only momentarily interrupted by the occurrence of one or more hot flame re-ignition events, typically lasting less than 1.0 s. The re-ignition event is initiated from a small region on the spherical surface that is eventually defined by a fully enveloping, re-ignited hot flame. This re-ignited high temperature flame has a diameter significantly larger than the preceding high temperature flame which had previously radiatively extinguished. An example of this re-ignition is provided in Figure 5 where a sequence of images taken 0.066 s apart shows the re-ignition kernel and the resulting flame wrapping around the contour of a spherical shell, presumably defining the stoichiometric surface. The re-ignited high temperature flame is not sustainable because, as with the original flame, its hypothetical flame radius without radiative loss exceeds that radius at which radiation loss exceeds heat generation.

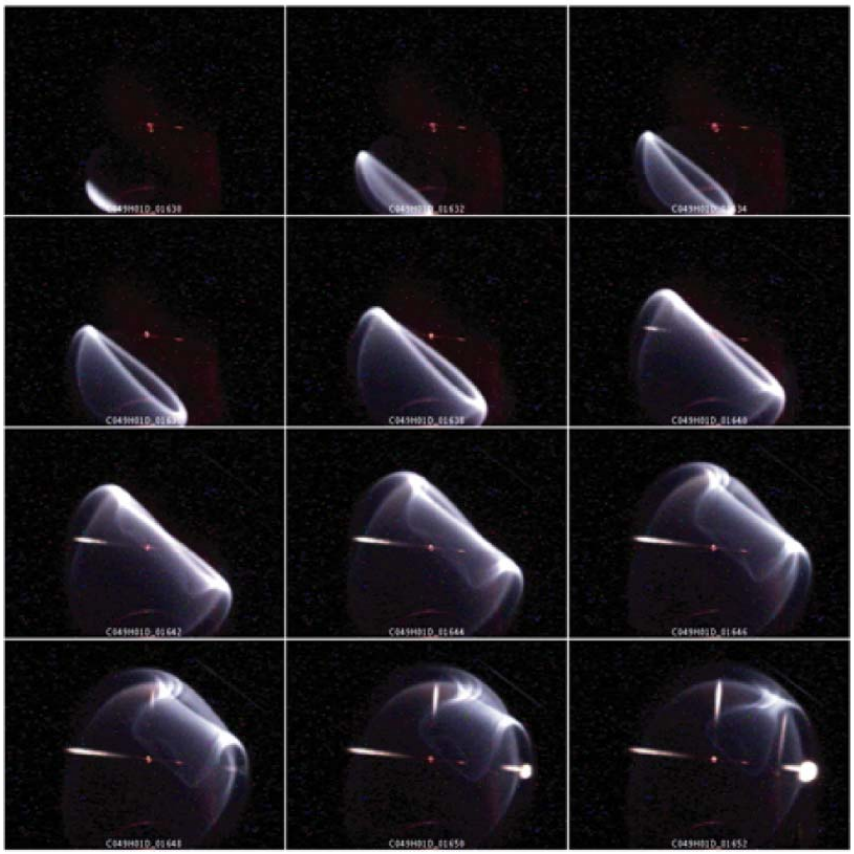

Fig. 5. Images showing the first of two spontaneous re-ignitions following a *second stage* combustion phase lasting approximately 10 s where no visible flame existed. Images in sequence are spaced 0.066 s apart and the total duration of the re-ignited hot flame is approximately 0.8 s. (d_o = 4.08 mm, 0.21 X_{O2}, 0.75 $X_{CO2,}$/balance N_2, 3 atm)

Figure 6 shows the predicted droplet diameter and flame diameter evolution along with the experimental measurements. The experimental conditions are d_o = 4.08 mm, 0.21 X_{O2}, 0.75 $X_{CO2,}$/balance N_2, at three atmosphere pressure. It can be seen that the predictions from the model agree favorably with the experimental measurement and captures all of the qualitative trends of the intricate features; especially the mutli-cycle two stage burning. The predicted droplet diameter regression rate is slower in comparison to the experiment. Likely experimental sources that may perturb the spherosymmetric result include slow gas/drop convection as a result of residual droplet drift [8] and movement along the tethering fiber, both of which may affect burning rate and the incomplete spherical flame structure/oscillatory behavior noted during transitions from low temperature burning to the second hot burning phase. It is apparent that in comparison to the atmospheric pressure experiments (Figure 1) the measured droplet diameter regression rates at elevated pressures show significantly greater departures from the local time averaged values. There exist multiple non-linear regimes in the droplet diameter regression rates. The flame diameter evolution presented in Figure 6b shows an example of this dynamic behavior. Initially the flame diameter is found to be large and together with the peak temperature evolution it is indicative of high temperature burning. Following the initial high temperature burn, the flame diameter is observed to decrease rapidly as a result of radiative heat loss, and transitions to the first low temperature/"*Cool Flame"* mode. Three subsequent initiations of transient hot flame burning of very short duration are each followed by a longer duration, "*Cool Flame"* burning period. In every *hot-cool flame* transition, the flame diameter is found to decrease by ~ 40- 50% of the prior cycle, maximum hot flame radius. Based on the predicted flame diameter evolution, the first transition to "*Cool Flame"* (i.e. visible flame extinction) is observed at t = 2.4 s, the first re-ignition at t_b = 4.64 s, the second and the third/last re-ignition

occuring at t_b = 14.56 s and t_b = 21.64 s. The predicted onset of second and third re-ignition that coincides with the experimentally observed 'first' and 'second' cases differs by ~ 2 s. However, the difference between the predictions and measurements during the very early stages ($0 \le t_b \le 5.0$ s) are likely the result of non-idealities in experiment and modeling of the experimentally aspherical, but symmetric hot wire ignition energy addition method. The initial ignition energy is known to significantly affect the transient establishment of the initial high temperature burning phase [9].

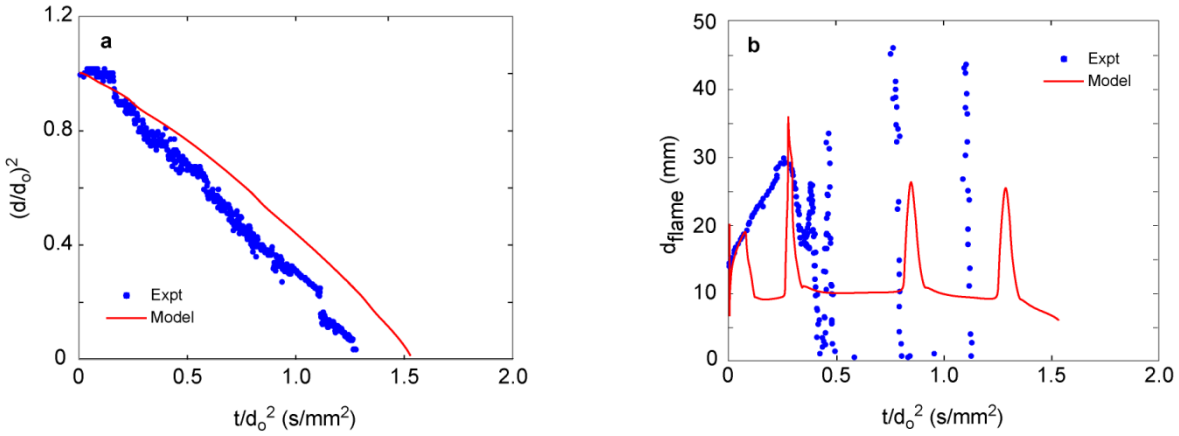

Figure 6. Measured and predicted evolution of: (a) droplet diameter and (b) flame diameter for a *n*-heptane droplet combustion. (d_o = 4.08 mm, 0.21 X_{O2}, 0.75 X_{CO2}/balance N_2, 3 atm).

4. Concluding Remarks

n-heptane droplet combustion under microgravity conditions has been successfully simulated using a recently developed transient spherosymmetric droplet combustion model. The simulation showed unique two stage "Cool Flame" like combustion behavior for large sized droplets. Unlike classical "Cool flames" these two stage combustion initiates at the high temperature combustion and then transitions to the "Cool flame" combustion process. The predictions from the simulations were found to be in good qualitative agreements with the experimental measurements The simulation results further indicated that heat losses initiates the two-stage behavior.

Acknowledgements

The work was supported by the National Aeronautics and Space Administration (NASA) through Grant Number NNX14AG461A.

References

[1] D. Dietrich, "Detailed results from the flame extinguishment experiment (FLEX)," *Technical Publication NASA/TP-2013-216046*, vol. NASA, Glenn Research Center, Cleveland OH 44135, USA, December 2013, 2013.
[2] T. I. Farouk and F. L. Dryer, "On the extinction characteristics of alcohol droplet combustion under microgravity conditions - A numerical study," *Combustion and Flame*, vol. 159, pp. 3208-3233, 2012.
[3] T. Farouk and F. L. Dryer, "Microgravity Droplet Combustion:Effect of Tethering Fiber on Burning Rate and Flame Structure," *Combustion Theory and Modelling*, vol. 15, pp. 487-515, 2011.
[4] T. Farouk and F. L. Dryer, "Tethered methanol droplet combustion in carbon-dioxide enriched environment under microgravity conditions," *Combustion and Flame*, vol. 159, pp. 200-209, 2012.
[5] M. Chaos, A. Kazakhov, Z. Zhao, and F. L. Dryer, "A high-temperature chemical kinetic model for primary reference fuels," *Int. J. Chem. Kinet.*, vol. 39, pp. 399-414, 2007.
[6] A. J. Marchese and F. L. Dryer, "The effect of non-luminous thermal radiation in microgravity droplet combustion," *Combustion Science and Technology*, vol. 124, pp. 371-402, 1997.
[7] H. J. Curran, P. Gaffuri, W. J. Pitz, and C. K. Westbrook, *Combustion and Flame*, vol. 114, pp. 149-177, 1998.
[8] M. Y. Choi, F. L. Dryer, and J. Haggard, "Observations of a slow burning regime for hydrocarbon droplets: n-heptane/air results,"

Proceedings of the Combustion Institute, vol. 23, pp. 1597 - 1604, 1990.

[9] T. Farouk, Y. C. Liu, A. J. Savas, C. T. Avedisian, and F. L. Dryer, "Sub-millimeter sized methyl butanoate droplet combustion: microgravity experiments and detailed numerical modeling," *Proceedings of the Combustion Institute*, vol. 34, pp. 1609 - 1616, 2013.